Construction of PROTAC-Mediated Ternary Complex Structure Distribution Profiles Using Extensive Conformational Search

Genki Kudo[1†], *Takumi Hirao*[2,3†], *Ryuhei Harada*[4], *Yasuteru Shigeta*[4], *Takatsugu Hirokawa*[3,5], *Ryunosuke Yoshino*[3,5*]

[1] Physics Department, Graduate School of Pure and Applied Sciences, University of Tsukuba, 1-1-1 Tennodai, Tsukuba 305-8571, Ibaraki, Japan.

[2] Doctoral Program in Medical Sciences, Graduate School of Comprehensive Human Sciences, University of Tsukuba, Tsukuba, Ibaraki, 305-8575, Japan.

[3] Division of Biomedical Science, Faculty of Medicine, University of Tsukuba, 1-1-1 Tennodai, Tsukuba, Ibaraki, 305-8575, Japan.

[4] Center for Computational Sciences, University of Tsukuba, 1-1-1 Tennodai, Tsukuba, Ibaraki, 305-8577, Japan.

[5] Transborder Medical Research Center, University of Tsukuba, 1-1-1 Tennodai, Tsukuba 305-8577, Ibaraki, Japan.

[*] To whom correspondence should be addressed.

† The authors wish it to be known that, in their opinion, the first two authors should be regarded as joint First Authors.

KEYWORDS: target protein degradation, PROTAC, E3 ubiquitin ligase, molecular dynamics simulation, PaCS-MD

ABSTRACT

Proteolysis-targeting chimeras (PROTACs) are heterobifunctional small molecules that recruit E3 ubiquitin ligases to a target protein and induce its ubiquitination by forming a ternary complex. For rational PROTAC design, computational methods that provide molecular insights into these association structures are required. In this study, we attempted extensive conformational search of PROTAC-mediated ternary complex structures using enhanced conformational sampling methods. Stable conformations were extracted from the molecular dynamics' ensembles by constructing Markov state models as their distribution profiles. These insights provided rational structure–activity relationships for PROTACs through the protein-ligand interaction analysis and the modeling of the ubiquitination system.

Introduction

More than 90% of global sales in the current drug market involve conventional small-molecule drugs.[1] Most small-molecule drugs have a high affinity for their targets and function by occupying hydrophobic pockets, limiting the application of conventional modalities for proteins with non-enzymatic functions, targets without hydrophobic pockets, and proteins with high affinity for their substrates.[2,3] Proteolysis-targeting chimeras (PROTACs) are a promising new class of molecules that function via "event-driven pharmacology," unlike the "occupancy-driven pharmacology" of conventional small molecules.[4–7] PROTACs, which are heterobifunctional small molecules, recruit E3 ubiquitin ligases to the target protein and induce its ubiquitination by forming a ternary complex. Polyubiquitinated target proteins are degraded by the ubiquitin-proteasome system (UPS). Target protein degradation (TPD) via PROTAC enables one to regulate of "undruggable" target protein levels.[2,6] Several PROTACs have recently been designed for drug development.[8–15]

During the formation of the ternary complex, the E3 ligand and warhead in the PROTAC substructures bind to the E3 ligase and target protein, respectively. These ligands determine the affinity of the PROTAC for proteins, and these substructures can be identified using approaches similar to those used for traditional small-molecule drugs, such as virtual screening and high-throughput screening.[16] The linker, another substructure in PROTAC, connects the E3 ligand and the warhead, and a suitable linker allows the formation of a productive ternary complex for ubiquitination.[17,18] In addition, the length and composition of the linker affect the positive cooperative assembly of the ternary complex and the target selectivity.[19–21] Despite the vital role of the linker in PROTAC activity, the design of the linker is challenging because the combination of ligands and the linker leads to optimal degradation.[7]

Since TPD activity requires stable protein–protein interactions with the linker, modeling ternary complexes accelerates PROTAC linker design.[19–21] Using the structure–activity relationships of PROTACs predicted from the modeled structures, the number of linker designs can be reduced to accelerate the development of PROTACs. However, the existing structural information on ternary complexes with PROTACs is limited, and simulation-based modeling methods are required. Michael et al. proposed four ensemble methods to predict ternary complexes by combining protein–protein docking and linker conformation analysis.[22] Rosetta-based structural predictions have also been reported,[23] successfully reproducing known ternary complex crystal structures. Although other ternary complex predictions and Rosetta-based rescoring have been reported,[24–26] Schiemer et al. characterized an ensemble of BTK-PROTAC-CIAP1 ternary complexes in solution using HSQC NMR, X-ray structural analysis, and computational modeling.[27] These results show that the target protein binds to E3 via PROTACs and has multiple conformations. This suggests that the linker's regulation of the ternary complex, proper lysine recognition, and ubiquitin transfer affect the affinity and kinetics. Therefore, for rational PROTAC linker design, predicting the ternary complex structure using only the known crystal structure, as in previously reported methods, is insufficient.[26] Consequently, a comprehensive search for stable ternary complex structures and the distribution profiles between these structures is needed to evaluate and understand the basis of PROTAC activity.

In this study, for three PROTACs with different linker lengths and degradation activities, we investigate possible conformations of the PROTAC-mediated ternary complexes using the hybrid conformational search[28] based on the parallel cascade selection molecular dynamics (PaCS-MD)[29] and the outlier flooding method (OFLOOD).[30,31] Distribution profiles from the free-energy landscape (FEL) and stable conformations at global/local minimum states were obtained on the

basis of the Markov state model (MSM) of the sampled conformational subspace. An extensive structural search of ternary complexes revealed multiple promising stable structures, providing essential insights into the induction of ubiquitination and rational structure–activity relationships for PROTACs.

Materials and methods

System setup of PROTAC systems

This study involved the conformational search of Von Hippel-Lindau tumor suppressor (VHL)-second bromodomain of bromodomain-containing protein 4 ($BRD4^{BD2}$)-PROTAC systems. We used MZ1, MZ2, and MZ4, which induce $BRD4^{BD2}$ degradation mediated by VHL and $BRD4^{BD2}$.[32] The E3 ligands and warheads of the three PROTACs had common structures, while the linker length differed for each PROTAC (Figure 1 and Table 1). Column 3 in Table 1 shows the degradation activities of the PROTACs, which was experimentally estimated by Chan et al.[32] While MZ1 with a medium linker length showed the best activity among the three PROTACs, the activity of MZ2 with a long linker was lower than that of MZ1. Moreover, MZ4, which had a short linker, exhibited the lowest activity among the PROTACs. The 3D structure of the ternary complex formed via MZ1 has been reported (Protein Data Bank [PDB] ID: 5T35); however, complexes formed via MZ2 and MZ4 have not yet been reported.

A setup for molecular dynamics (MD) simulation of the PROTAC systems was developed. First, an initial structure with a PROTAC extension was prepared. Based on the crystal structure of MZ1, a model was generated by manually altering the dihedral angle of the linker substructure to 180 degrees using GaussView,[33] as shown in Figure S1 in the Supporting Information. Next, each initial model was placed in a rectangular box with a margin of 10 Å from the proteins, and the box was filled with water molecules. Na^+ and Cl^- ions were added to neutralize the system. The force fields of the proteins and water molecules were set to the amber ff14SB and TIP3P model, respectively.[34,35] For the PROTACs, the restrained electrostatic potential procedure (RESP) was employed to fit and convert the partial charges to reproduce the electrostatic potential, which was calculated using Gaussian 16 Rev C.01.[36] The electrostatic potential was calculated at the HF/6-

31G level using an extended PROTAC structure. The force fields of the PROTACs were derived using the general AMBER force field (GAFF).[37] These system constructions were performed using the antechamber and leap module of AmberTools20.[38] Each prepared system was minimized for 10000 steps using the steepest descent algorithm. The minimized system was gradually heated to 300 K during a 100-ps *NVT* MD simulation with harmonic position restraints on the heavy solute atoms (force constant, 10 kcal/mol/Å^2). After the *NVT* equilibration, the *NPT* MD simulation was performed at 300 K and 1 bar for 800 ps with a gradual reduction in the position restraints from 10 kcal/mol/Å^2 to 0 kcal/mol/Å^2. The constraint algorithm was set as the LINCS algorithm[39] to increase time step of 2 fs. The velocity-rescaling thermostat and Berendsen barostat were set to control the temperature and pressure, respectively.[40–43] The version of GROMACS2021.5 was used for all MD simulations in this study.[44]

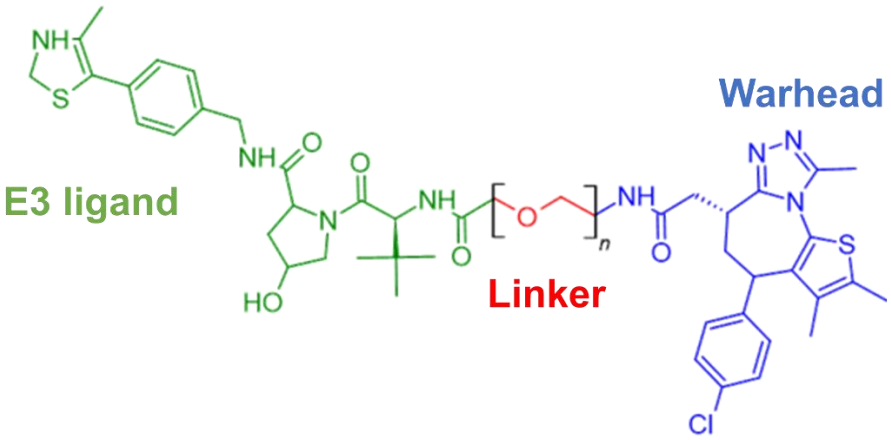

Figure 1. Common structure of PROTACs

Table 1. PROTAC information

PROTAC	Linker length (*n*)	pDC_{50}	PDB
MZ1	Medium (*n* = 3)	8.6	5T35

MZ2	Long (n = 4)	8.0	N.D.
MZ4	Short (n = 2)	7.0	N.D.

Hybrid conformational search based on PaCS-MD and OFLOOD

PaCS-MD is a rare-event sampling method without any extra bias in the MD simulation.[29] PaCS-MD repeats multiple MD simulations and selects restart structures for efficient conformational sampling. Restarting structures were selected on the basis of the specified reaction coordinates (RCs) of the MD trajectories. The sampling efficiency of PaCS-MD depends on the selection of appropriate RCs. In previous studies using PaCS-MD, a wide variety of biomolecule descriptors, such as the distance between two domains and the root mean square deviation (RMSD) with respect to a known structure, were selected as RCs.[29,45–47] Additionally, the hybrid conformational search[28] based on the combination of PaCS-MD with OFLOOD enables the search for a broad configurational space.[47,48] The OFLOOD method detects outliers among the MD trajectories based on the reaction coordinate space and resamples starting from these outliers.[30] Similar to PaCS-MD, the sampling efficiency of OFLOOD depends on selecting of an appropriate reaction coordinate space.[49,50]

This study used PaCS-MD and OFLOOD for each PROTAC system to perform the hybrid conformational search. Our method was divided into two steps: PaCS-MD based on the Cα-RMSD and OFLOOD. First, PaCS-MD was performed starting from the initial model with the setup. For each cycle in PaCS-MD, 100-ps MD simulations were run in parallel with 10 conformations at different initial velocities. After multiple MD simulations, the Cα-RMSD values with respect to the crystal structure of VHL-MZ1-BRD4^{BD2} (PDB ID: 5T35) of the snapshots were calculated, and 10 snapshots with low Cα-RMSD values were selected as restart structures for the next cycle.

This process was repeated for 100 times as the first step. Second, OFLOOD was performed based on the MD trajectories obtained in the first step. Two RCs were selected for OFLOOD (Figure 2): the distance between the centroids of VHL and $BRD4^{BD2}$ and the dihedral angle forming VHL and $BRD4^{BD2}$. The dihedral angle was defined using the Cα atom of Trp117 in VHL, centroid of VHL, centroid of $BRD4^{BD2}$, and Cα atom of Arg423 in $BRD4^{BD2}$. Two Cα atoms were selected because root-mean-square fluctuation (RMSF) of these residues was stable in the pre-conventional MD simulation (Figure S2). In the OFLOOD cycle, starting from snapshots that were detected as outliers using FlexDice,[51] 100-ps MD simulations were run in parallel with 10 conformations at different initial velocities. Note that outliers with a distance over 51 Å were excluded from the restart structures because these structures may dissociate proteins and PROTACs. The OFLOOD cycle was repeated for 150 times. For each PROTAC system, the total computational time of the hybrid conformational search was 250 ns.

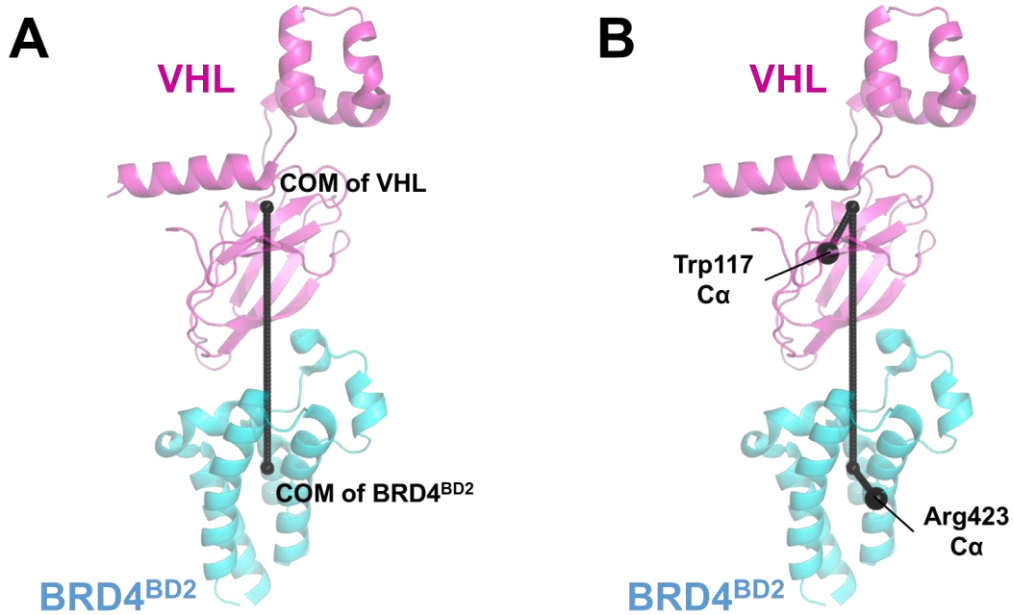

Figure 2. Reaction coordinates specified in OFLOOD

A. Distance between the centroids of the proteins. B. Dihedral angle defined in the proteins. VHL and $BRD4^{BD2}$ are colored in magenta and cyan, respectively.

Free-energy landscape construction based on the MSM

MSMs were constructed to evaluate the conformations of the PROTAC systems quantitatively. The construction of MSMs enable one to calculate FELs of the sampled MD trajectories.[52] To construct reliable MSMs, the conformational resampling was performed using the snapshots sampled by the hybrid conformational search. Specifically, multiple conformations were selected from the grids on the distance-dihedral subspace searched by the present method, which each grid was generated per 1 Å and 15 degrees. Here, snapshots close to each grid were selected as the initial structures of the conformational resampling. For the complex systems with MZ1/2/4, 409/351/351 snapshots were selected as the initial structures of the additional MD simulations. Subsequently, 50-ns conventional MD simulations were performed for each initial structure, and snapshots were recorded per 100 ps. In summary, the total simulation time per system was approximately 17.5-20.5 μs. After the conformational resampling through the additional MD simulations, the snapshots were clustered into 100 microstates based on *k*-means clustering. For these microstates, the transition matrix (T_{ij}) was estimated by counting structural transitions between microstates *i* and *j*. The lag time required to estimate the transition matrix was set to 5 ns. Subsequently, a stationary distribution (π_i) was generated from the transition matrix. Finally, the FEL of microstate *i* was calculated as follows:

$$F_i = -k_B T \ln \frac{\pi_i}{\max_j \pi_j} \quad (1)$$

where k_B and T are the Boltzmann constant and absolute temperature, respectively. The FEL to quantitatively evaluate of the conformation of each PROTAC system is depicted based on the calculated free energies. PyEMMA was used for the FEL construction.[53]

Analysis of ternary complex structures

Stable ternary complex structures were extracted based on the FEL of each PROTAC system. Complex structures at the global and local minimum states in the FEL were selected, and their Cα-RMSD values were compared with those of the crystal structure with MZ1 (PDB ID: 5T35). A total of 100 structures around these minimum states were extracted to determine the binding free energy using the generalized Born and surface area continuum solvation method (MM/GBSA).[54] We calculated the binding free energy for the PROTACs in VHL-BRD4^{BD2} (ΔG_{bind}^{PROTAC}) and protein–protein interactions without the PROTACs (ΔG_{bind}^{PPI}). The gmx_mmpbsa tool was used for the binding free-energy calculations.[55]

Results

Hybrid conformational search based on PaCS-MD and OFLOOD

Figure 3 shows Cα-RMSD profiles of structural transitions extracted by the PaCS-MD simulations. The Cα-RMSD of each system versus cycle is shown in Fig. 3A. Note that for each plot, the minimum Cα-RMSD value in each cycle was plotted in this figure. The complex structures at cycles 0 (initial), 10, 20, and 100 in each system are shown in Fig. 3B-3D. All systems showed RMSD values rapidly decreasing below 4 Å within the 20 cycles. This rapid decrease was attributable to the structural flexibility of these transition states, which are only joined by PROTACs and do not have protein–protein interactions. The details of the transition states in the simulations are presented in Fig. S3. These structural transitions stagnate the interacting proteins, and these systems have an RMSD of approximately 1 Å. Although MZ1 and MZ4 showed a monotonic decrease in RMSD until the 20-30th cycle, MZ2 showed two stalls from the 10-30th cycle and above the 40th cycle during the PaCS-MD simulations. This corresponds to the linker in MZ2 searching for a stable position during the first stall.

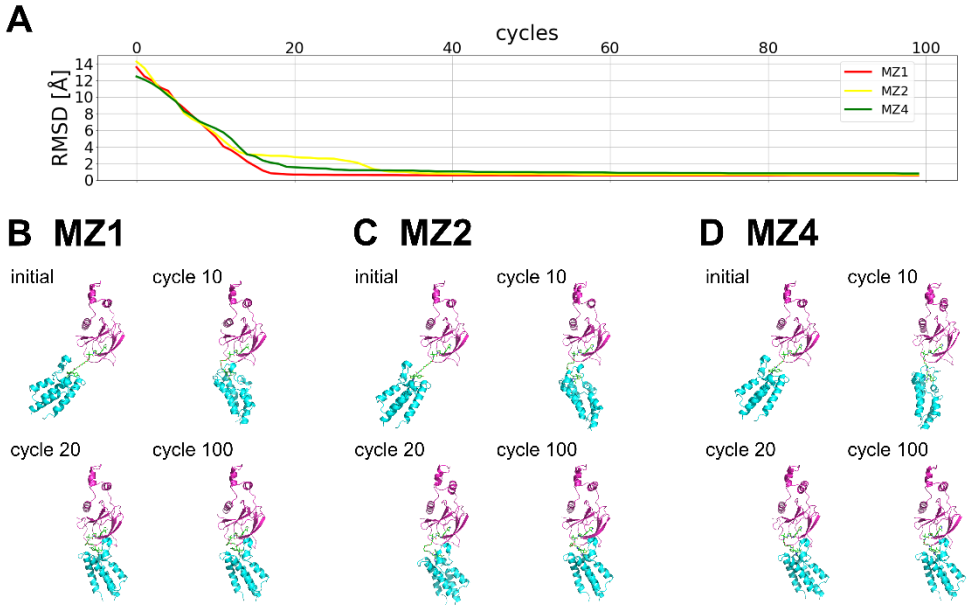

Figure 3. Structure transition in the PaCS-MD simulations characterized by Cα-RMSD.

A. The minimum Cα-RMSD values versus the PaCS-MD cycles for the PROTAC systems. The profiles of MZ1/2/4 are colored in red, yellow, and green, respectively. B-D. Structural transitions of the ternary complexes for MZ1/2/4 during PaCS-MD cycles. The structures of VHL, $BRD4^{BD2}$, and PROTAC are colored in magenta, cyan, and green, respectively.

For the further conformational search of the PROTACs, OFLOOD was subsequentially performed based on the PaCS-MD trajectories. Figure S4 presents the extension of the subspace searched by OFLOOD according to the cycle. After the 150 OFLOOD cycles, a broad conformational subspace was searched for each system, allowing one to construct reliable MSMs to calculate FELs. Figure 4 shows the FEL of each PROTAC system. The FEL of MZ1 had a single global minimum state with multiple local minimum states. In contrast, the FEL of MZ2 also had a single global minimum state with widely distributed multiple local minimum states. In the FEL of MZ4, an area with a free energy value of less than 2 k_BT was widespread, and two minimum

regions were observed. These results indicated that MZ1 and MZ2 predominantly mediate a single stable ternary complex structure, whereas MZ4 can mediate multiple stable structures.

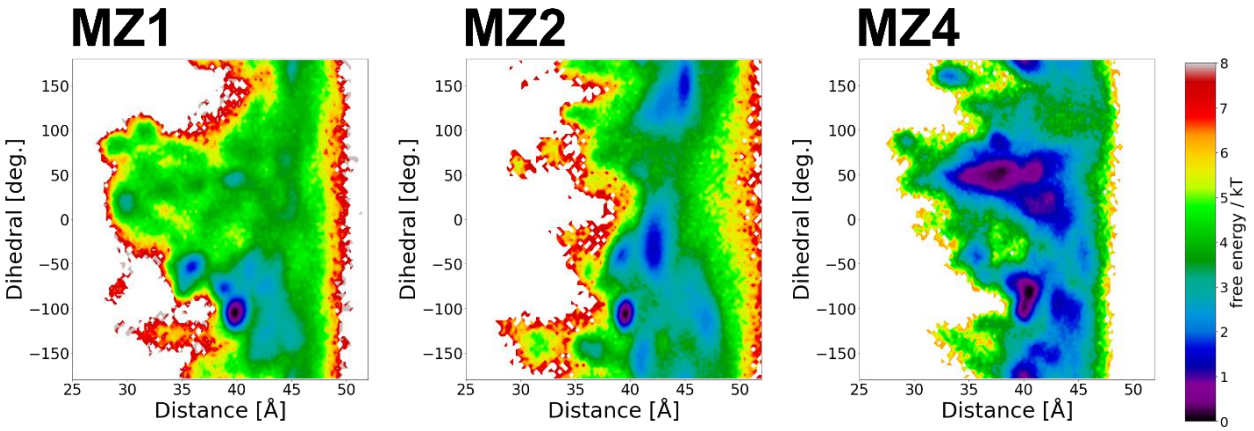

Figure 4. Free-energy landscapes of PROTAC systems.

The FEL of each PROTAC system mapped to each 2D space. The areas with high/low free-energy values are highlighted in warm/cool colors.

Structural evaluation of stable conformations

Ternary complex structures at the global and local minimum states were extracted for each PROTAC system. The whole complex structures and binding poses are shown in Figure 5 and S5, respectively. Structural evaluation was performed based on RMSD and binding free-energy values for each state, as shown in Table 2. For the system with MZ1, the global minimum state was picked up at approximately [39.95, -105.73] in the FEL. This structure had a low Cα-RMSD (1.329 Å) with respect to the crystal structure. Moreover, the RMSD of the heavy atoms in MZ1 was 0.838 Å. These results indicated that present method worked correctly to predict the ternary complex structure as a global minimum state. The local minimum state of the MZ1 system was at

approximately [35.92, -56.89]. This state had a higher Cα-RMSD (5.303 Å) and PROTAC-RMSD (1.911 Å) than the global minimum state. This indicated that the local minimum state differed significantly from the global minimum state and crystal structure. In addition, the binding free energy (ΔG_{bind}^{PPI}) in the proteins of the local minimum state was more than 12 kcal/mol inferior to that of the global minimum state. Since this local minimum state showed a high free-energy value in the FEL and inferior binding free energy between the proteins, this state was an unstable conformation compared to the global minimum state, meaning that the global minimum state existed predominantly as an MZ1-mediated ternary complex.

Next, the stable ternary complex structures with MZ2 were extracted. The global minimum state was picked up at approximately [39.15, -106.12] in the FEL. This state had a low Cα-RMSD, 1.118 Å, similar to the global minimum state in MZ1 and the crystal structure. The binding free energy of the PROTAC was -98.45 ± 5.33 kcal/mol, which is slightly inferior to that of the global minimum state with MZ1. The local minimum state in MZ2 picked up at approximately [41.69, -31.17] had a different conformation from the crystal structure and the global minimum state in MZ2. This local minimum state showed no protein–protein interactions and had a hydrogen bond between the linker and Arg69 in VHL. Actually, ΔG_{bind}^{PPI} at the local minimum state of MZ2 was considerably inferior to that at the global minimum state; the value was -6.44 ± 7.29 kcal/mol. These results indicated that the local minimum state in the MZ2 system was relatively more unstable than the global minimum state. Consequently, the MZ2 system had a dominant global minimum state, with a conformation similar to that of the crystal structure. Finally, the ternary complexes with MZ4 were analyzed. Similar to MZ1 and MZ2, the global minimum state was picked up at approximately [40.44, -88.08] and it was similar to the crystal structures; the Cα-RMSD value was 1.537 Å. On the other hand, the local minimum state was picked up

approximately at [37.77, 48.81] and it differed from the crystal structure and the others. The local minimum showed a larger RMSD value and a significantly shifted dihedral angle compared to the global minimum state. However, this local minimum state had an affinity for proteins; the value was -20.13 ± 9.59 kcal/mol. This affinity was equivalent to that of the global minimum state. Electrostatic interactions are formed in the local minimum state. This indicated that the local minimum state in the MZ4 system was as stable as the global minimum state. This distribution profile in the MZ4 system is distinctive and unlike those in the MZ1 and MZ2 systems. 3D views of the entire model and the binding sites of these ternary complex structures are provided in the Supporting Information.

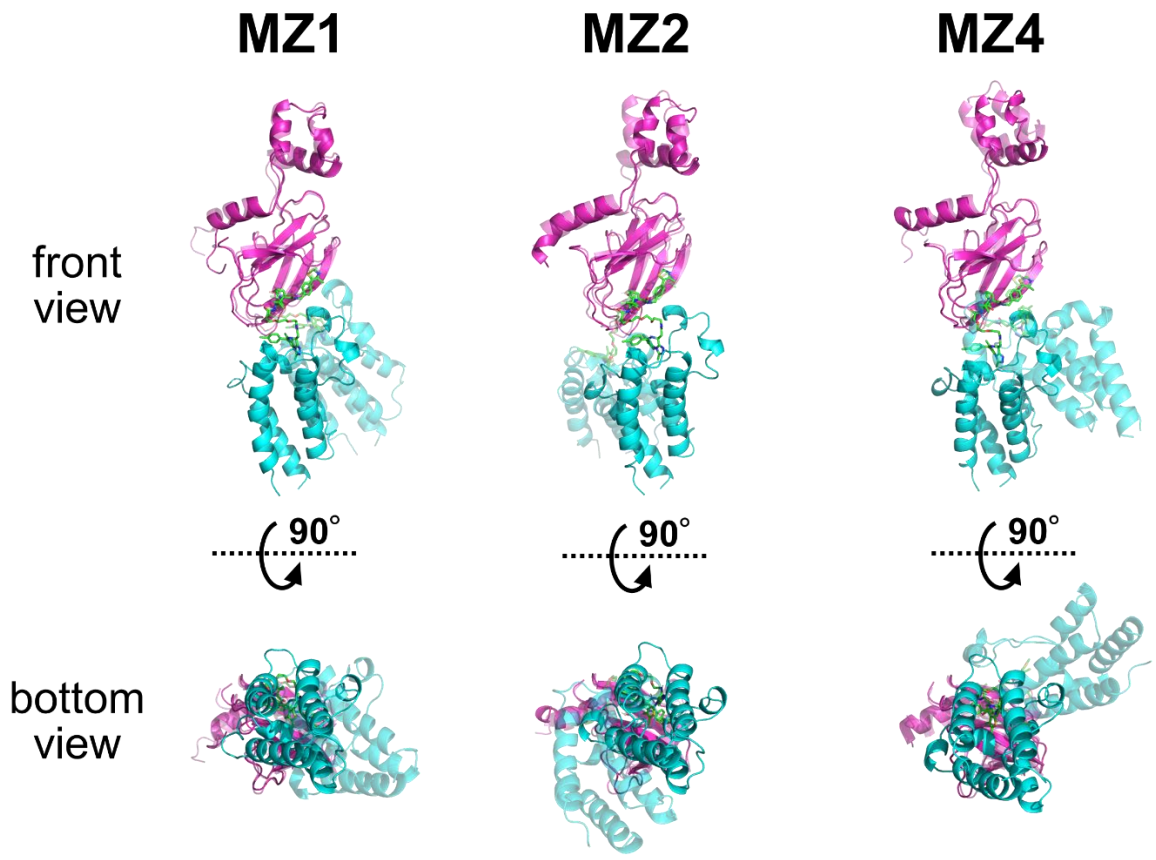

Figure 5. Ternary complex structures of the global and local minimum states in each system.

VHL, $BRD4^{BD2}$, and PROTACs are shown in magenta, cyan, and green, respectively. For each PROTAC system, the complex structures at the global and local minimum states are shown as opaque and semitransparent models, respectively.

Table 2. Details of ternary complex structures for the global/local minimum

PROTAC	Minimum	Cα-RMSD with 5T35	ΔG_{bind}^{PROTAC} [kcal/mol]	ΔG_{bind}^{PPI} [kcal/mol]
MZ1	Global [39.95, -105.73]	1.238 Å	-103.99 ± 4.43	-25.74 ± 5.91
	Local [35.92, -56.89]	5.255 Å	-105.43 ± 5.64	-12.94 ± 8.08
MZ2	Global [39.15, -106.12]	1.118 Å	-98.45 ± 5.33	-24.46 ± 6.67
	Local [41.69, -31.17]	6.035 Å	-99.55 ± 8.73	-6.44 ± 7.29
MZ4	Global [40.44, -88.08]	1.537 Å	-100.49 ± 5.85	-25.42 ± 7.72
	Local [37.77, 48.81]	11.376 Å	-99.47 ± 7.80	-20.13 ± 9.59

Discussion

Distribution profiles of PROTACs

The FELs and stable ternary complex structures of the three PROTAC systems were obtained using our method (Figures 4 and 5). Quantitative evaluation of these stable conformations enabled the estimation of their distribution profiles (Figure 4 and Table 2). The global minimum state of the MZ1 system was dominant because its FEL had a funnel shape, and the binding free energies were higher than those of the local minimum state. The MZ2 system also showed a dominant global minimum state because this conformation was more stable than the others in the system. Notably, despite the differences in the linker lengths of the PROTACs, the whole conformations of these global minimum states were similar (Figures 5, S5, and S6). The global minimum state of the MZ4 system had a similar conformation to that of the dominant state in the MZ1 and MZ2 systems. In addition, the local minimum state of the MZ4 system was as stable as the global minimum state because of the equivalent free energy, as estimated by the FEL, and binding free energy, based on MM/GBSA. In summary, PROTACs with extensive degradation activity have a distribution profile with a common conformation similar to the crystal structure, even if they show differences in linker length.

Structural analysis based on linker lengths

For the MZ1 and MZ2 systems, despite showing different linker lengths and degradation activities, their distribution profiles were similar each other because the system had a dominant stable conformation. Their most stable conformations were also similar (Figure 5 and Table 2). To understand the structure–activity relationship of the MZ1 and MZ2 systems, a protein-ligand

interaction fingerprint (PLIF) analysis of these conformations was performed. The PLIF tool, which was implemented in the Molecular Operating Environment (MOE) software, represents the interaction between a compound and each amino acid residue in a protein as a fingerprint bit, according to its interaction type. One hundred snapshots around the global minimum in each FEL were used for the PLIF analysis. Subsequently, a significance analysis was performed based on the fingerprints obtained from the global minimum for each PROTAC system. Figure 6A shows a fingerprint comparison of the global minimum states of MZ1 and MZ2. The findings indicated that the contacts with His437, Glu438, and Val439 in $BRD4^{BD2}$ were specific to the global minimum state for MZ1, and the contact with His110 in VHL was specific to the global minimum state for MZ2 (Figures 6B and 6C). The difference in the interactions indicates that conformations with MZ1 and MZ2 have a slight difference in the binding site, whereas the whole structures are similar. These analyses indicated that the interfaces of the ternary complexes in the MZ1/2 systems were different. In fact, in comparison with the global minimum conformation in the MZ1 system, the target protein of the global minimum conformation in the MZ2 system was slightly shifted (Figure S6, morphing movie in Supporting Information). Focusing on the conformation at the global minimum state in the MZ1 system, the space around the linker was too small to place a long linker such as that of MZ2. Consequently, the target protein at the global minimum state in the MZ2 system was forced to shift such that its space could expand, even if the shift caused a loss of interactions between the protein and PROTAC. This analysis suggests that the long linker length in MZ2 causes a loss of affinity for the ternary complex (column 4 in Table 2) and decreases the activity of the target degradation.

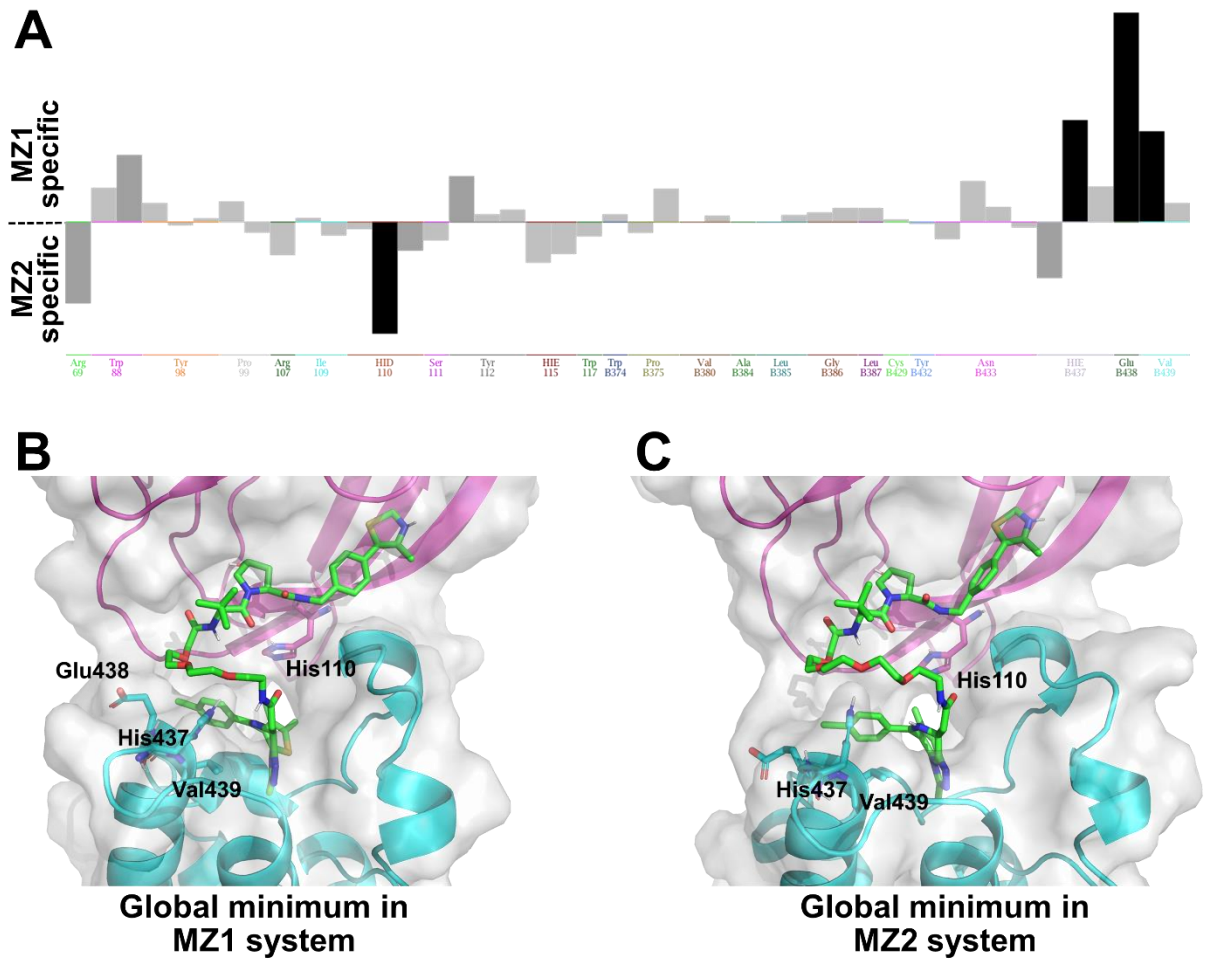

Figure 6. Comparison of the global minimum states in the MZ1 and MZ2 systems. A. Protein-ligand interaction fingerprints in the MZ1 and MZ2 systems. B-C. Binding poses of the global minimum states in MZ1 and MZ2 systems.

Ubiquitin accessibility of the ternary complexes

MZ4, a PROTAC with a short linker, showed lower degradation activity than MZ1 and MZ2, and our results showed that the distribution profile of the MZ4-mediated ternary complex had multiple stable conformations. To analyze the functional differences between these conformations, we modeled ubiquitination systems, including Elongin-B, Elongin-C, Cullin-2,

RBX1, E2 ligase, and ubiquitin (Figure 7). The structures from PDB IDs 5T35, 5N4W, 4P5O, and 1YIW were used to model the ubiquitination system (Figure 7A). Using this model, we evaluated whether the MZ4-mediated formation of the ternary complex promoted ubiquitination. The global minimum state with MZ1 and the local minimum state with MZ4 were aligned with VHL in the ubiquitination model. Subsequently, the distance between the cysteine in the active sites of the E2 ligase, which forms a thioester bond with ubiquitin, and the exposed lysine (K355, K368, K445, and K456) in the target protein was calculated. For the global minimum state with MZ1, the minimum distance between the cysteine and the exposed lysine was 34.2 Å (Figure 7B). In contrast, for the local minimum state with MZ4, the specific conformation in the MZ4 system, the minimum distance was 73.3 Å (Figure 7C). Thus, the ubiquitin accessibility of the local minimum state in the MZ4 system is lower than that of the global minimum state in the MZ1 system and the others. Since PROTACs function as drugs by inducing the ubiquitination of the target protein, a conformation with low ubiquitin accessibility is unsuitable for the ternary complex structure induced by PROTACs. Thus, these results suggest that MZ4 has a low degradation activity.

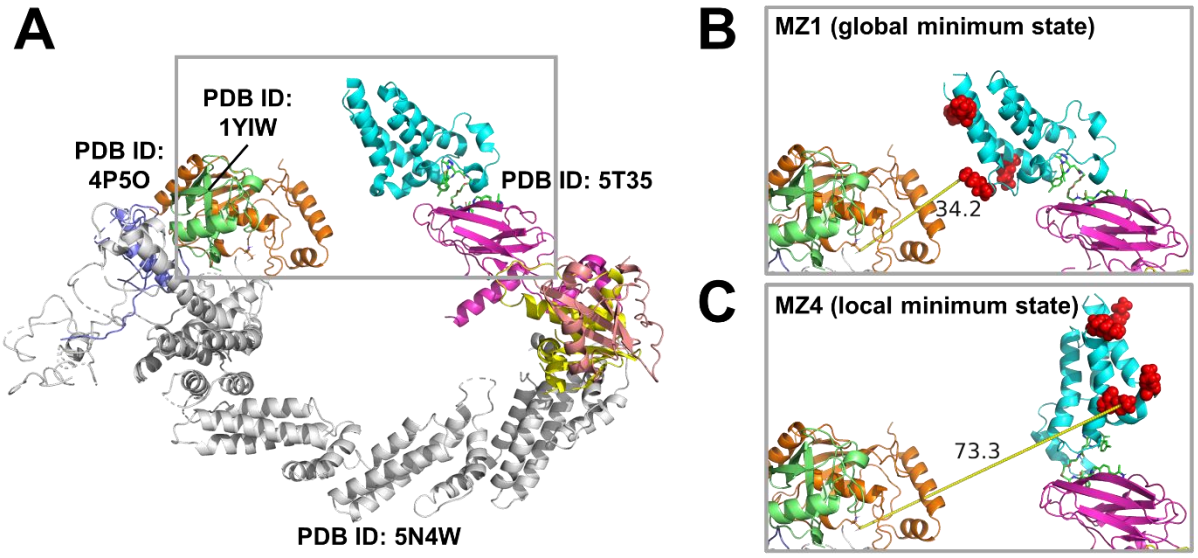

Figure 7. Modeling of the ubiquitination system and alignment with the global/local minimum state

A. Whole modeling structure consisting of Ub-Ubc12-Rbx1-Cul2-EloBC-VHL-BRD4^{BD2}. B. Aligned model with the ubiquitination model and the global minimum state with MZ1. C. Aligned model with the ubiquitination model and the local minimum state with MZ4. The exposed-Lys are shown as red spheres.

Structure-activity relationships based on distribution profiles

The structure-activity relationships with PROTACs were revealed on the basis of the distribution profiles of the ternary complexes. MZ1, the most promising inducer of the three PROTACs, had an FEL with a large funnel. The structure at the global minimum state in the funnel was similar to the crystal structure (PDB ID: 5T35). MZ2, which has lower activity than MZ1, had

a conformation similar to that of the global minimum state of MZ1. However, the PLIF analysis and structural comparison suggested that at the global minimum state with MZ2, the long linker reduces the affinity of the ternary complex by shifting its conformation in comparison with the global minimum state with MZ1. In other words, the low activity of MZ2 results in a long linker that regulates ternary complex associations.

MZ4, which has the lowest activity among the three PROTACs, has an FEL with two large funnels. Among the stable conformations in these funnels, one was similar to the global minima of other PROTACs and the other was MZ4-specific. According to structural evaluation using the ubiquitination system, the MZ4-specific conformation was unfavorable for the ubiquitination of the target protein. In summary, the low activity of MZ4 indicated that this anti-ubiquitinated conformation was distributed to the same extent as the global minimum state. Schiemer et al. reported that PROTAC-mediated target proteins and E3 bind flexibly to each other and form multiple ensembles.[27] Furthermore, Charlotte et al. revealed the cryo-EM structures of the VHL Cullin 2 RING E3 ligase complexed with MZ1, $Brd4^{BD2}$ and mentioned that one or more specific lysine residues must be favorably oriented to the catalytic site to promote highly specific and efficient ubiquitination.[56] Thus, exhaustive sampling in this study also suggests that proper linker design not only increases the affinity of PROTACs but also stabilizes the specific conformations that allow ubiquitination to proceed from among the multiple ensembles.

Conclusions

Although molecular insights into PROTAC activity are crucial for rational PROTAC design, computational studies on these complex structures are limited. Thus, we attempted

extensive conformational search of PROTAC-mediated ternary complex structures using the PaCS-MD and OFLOOD methods for three PROTACs with known degradation activities. The FELs obtained from the MD ensembles characterized the stable conformations of the ternary complex and their distribution profiles. While MZ1 and MZ2, which were PROTACs with medium and long linker lengths, respectively, had a dominant conformation, MZ4, with a short linker length, had multiple stable conformations. Detailed analysis of the MZ1 and MZ2 systems using PLIF indicated that the low degradation activity of MZ2 was attributable to the long linker twisting the ternary complex conformation and regulating these associations. In other words, the low activity of MZ2 was derived from a long linker that regulated ternary complex associations. Ubiquitination system modeling with MZ1 and MZ4 indicated that the MZ4-specific conformation is an unfavorable state for ubiquitination of the target protein because the lysine residue in $BRD4^{BD2}$ is far from the active site of ubiquitination. Hence, a high distribution of the specific conformation of MZ4 can result in low degradation activity. In summary, the present extensive conformational search and an understanding of the distribution profile can provide insights into the structure–activity relationships of PROTACs.

Data and software availability

3D structures of the proteins were downloaded from the Protein Data Bank (PDB). We used AmberTools20 and Gaussian 16 Rev B.01 for PROTAC preparation. AmberTools20 was used to prepare the MD system. GROMACS 2021.5 was used as the MD engine. PyEMMA was used to estimate MSM. Gmx_MMPBSA was used to calculate binding free energy based on the MM/GBSA method. PyMOL was used for visualization, Cα-RMSD calculation, and distance

measurement. MOE (Chemical Computing Group, LLC) was used for PLIF analysis. Data of the present study is available from the corresponding authors at a reasonable request.

ASSOCIATED CONTENT

The Supporting Information is available free of charge.

Figure S1: Initial models of each PROTAC system.

Figure S2: RMSF of the C α atom in VHL and BRD4BD2

Figure S3: Ternary complex structure transitions in PaCS-MD based on Cα-RMSD

Figure S4: Sampling transitions in the OFLOOD method

Figure S5: Binding modes of the global and local minima in each PROTAC system

Figure S6: Structural comparison of the global minimum states in the MZ1 and MZ2 systems

Entire view of global and local minimum states of each PROTAC system (MZ1/2/4_mediated _global/local_minimum_state.mp4)

Molecular morphing from MZ1-mediated global minimum state to MZ2-mediated global minimum state (morphing_from_MZ1_to_MZ2_system.mp4)

AUTHOR INFORMATION

Corresponding Author

*Ryunosuke Yoshino

Faculty of Medicine, University of Tsukuba, 1-1-1 Tennodai, Tsukuba 305-8575, Ibaraki, Japan; Transborder Medical Research Center, University of Tsukuba, 1-1-1 Tennodai, Tsukuba 305-8577, Ibaraki, Japan; orcid.org/0000-0002-5123-1349; Email: yoshino.r.aa@md.tsukuba.ac.jp

Author Contributions

G.K., T.Hirao, R.H., Y.S., T.Hirokawa, and R.Y. conceived the study. G.K., T.Hirao, R.Y., and T.Hirokawa selected the targeted PROTAC-mediated ternary complexes. G.K., T.Hirao, and R.H. implemented the PaCS-MD and OFLOOD methods. G.K. and T.Hirao performed the experiments and G.K. analyzed the data. The manuscript was written with contributions from all the authors. All authors approved the final version of the manuscript.

Funding Sources

This research was partially supported by the Research Support Project for Life Science and Drug Discovery [Basis for Supporting Innovative Drug Discovery and Life Science Research (BINDS)] (grant number JP23ama121029j0003) of the Japan Agency for Medical Research and Development (AMED), MEXT as “Program for Promoting Researches on the Supercomputer Fugaku” (Simulation- and AI-driven next-generation medicine and drug discovery based on "Fugaku", JPMXP1020230120), and KAKENHI (grant numbers JP23K16987, JP23H04879, JP23H02427, and JP23K18033) from the Japan Society for the Promotion of Science (JSPS).

Notes

The authors declare no competing financial interests.

ACKNOWLEDGMENT

PaCS-MD and OFLOOD uses the Cygnus computational resources provided by the Multidisciplinary Cooperative Research Program at the Center for Computational Sciences (Project Code: CADD) at the University of Tsukuba. Additional MD simulationfor MSM construction uses used computational resources of (supercomputer Fugaku provided by the RIKEN Center for Computational Science) (Project ID: hp230216). G.K. acknowledges the support for Grant-in-Aid for JSPS Fellows (grant numbers 24J11444) from the JSPS.

ABBREVIATIONS

$BRD4^{BD2}$, second bromodomain of bromodomain-containing protein 4; GAFF, general AMBER force field; FEL, free-energy landscape; MD, molecular dynamics; PaCS-MD, parallel cascade selection molecular dynamics; MSM, Markov state model; OFLOOD, outlier flooding; PDB, Protein Data Bank; PLIF, protein-ligand interaction fingerprint; PROTAC, proteolysis-targeting chimeras; RESP, restrained electrostatic potential procedure; RMSD, root mean square deviation; TPD, target protein degradation; UPS, ubiquitin-proteasome system; VHL, Von Hippel-Lindau tumor suppressor.

REFERENCES

(1) Makurvet, F. D. Biologics vs. Small Molecules: Drug Costs and Patient Access. *Med Drug Discov* **2021**, *9*, 100075. https://doi.org/10.1016/j.medidd.2020.100075.

(2) Békés, M.; Langley, D. R.; Crews, C. M. PROTAC Targeted Protein Degraders: The Past Is Prologue. *Nature Reviews Drug Discovery*. Nature Research March 1, 2022, pp 181–200. https://doi.org/10.1038/s41573-021-00371-6.

(3) Kelm, J. M.; Pandey, D. S.; Malin, E.; Kansou, H.; Arora, S.; Kumar, R.; Gavande, N. S. PROTAC'ing Oncoproteins: Targeted Protein Degradation for Cancer Therapy. *Molecular Cancer*. BioMed Central Ltd December 1, 2023. https://doi.org/10.1186/s12943-022-01707-5.

(4) Churcher, I. Protac-Induced Protein Degradation in Drug Discovery: Breaking the Rules or Just Making New Ones? *J Med Chem* **2018**, *61* (2), 444–452. https://doi.org/10.1021/acs.jmedchem.7b01272.

(5) Coleman, K. G.; Crews, C. M. Proteolysis-Targeting Chimeras: Harnessing the Ubiquitin-Proteasome System to Induce Degradation of Specific Target Proteins BACKGROUND INFORMATION. *The Annual Review of Cancer Biology is online at* **2018**, *2*, 41–58. https://doi.org/10.1146/annurev-cancerbio.

(6) Pettersson, M.; Crews, C. M. PROteolysis TArgeting Chimeras (PROTACs) — Past, Present and Future. *Drug Discovery Today: Technologies*. Elsevier Ltd April 1, 2019, pp 15–27. https://doi.org/10.1016/j.ddtec.2019.01.002.

(7) Troup, R. I.; Fallan, C.; Baud, M. G. J. Current Strategies for the Design of PROTAC Linkers: A Critical Review. *Exploration of Targeted Anti-tumor Therapy*. Open Exploration Publishing Inc 2020, pp 273–312. https://doi.org/10.37349/etat.2020.00018.

(8) Sakamoto, K. M.; Kim, K. B.; Kumagai, A.; Mercurio, F.; Crews, C. M.; Deshaies, R. J. *Protacs: Chimeric Molecules That Target Proteins to the Skp1-Cullin-F Box Complex for Ubiquitination and Degradation*; 2001. https://www.pnas.org.

(9) Powell, C. E.; Gao, Y.; Tan, L.; Donovan, K. A.; Nowak, R. P.; Loehr, A.; Bahcall, M.; Fischer, E. S.; Jänne, P. A.; George, R. E.; Gray, N. S. Chemically Induced Degradation of Anaplastic Lymphoma Kinase (ALK). *J Med Chem* **2018**, *61* (9), 4249–4255. https://doi.org/10.1021/acs.jmedchem.7b01655.

(10) Burslem, G. M.; Smith, B. E.; Lai, A. C.; Jaime-Figueroa, S.; McQuaid, D. C.; Bondeson, D. P.; Toure, M.; Dong, H.; Qian, Y.; Wang, J.; Crew, A. P.; Hines, J.; Crews, C. M. The Advantages of Targeted Protein Degradation Over Inhibition: An RTK Case Study. *Cell Chem Biol* **2018**, *25* (1), 67-77.e3. https://doi.org/10.1016/j.chembiol.2017.09.009.

(11) He, Y.; Khan, S.; Huo, Z.; Lv, D.; Zhang, X.; Liu, X.; Yuan, Y.; Hromas, R.; Xu, M.; Zheng, G.; Zhou, D. Proteolysis Targeting Chimeras (PROTACs) Are Emerging Therapeutics for Hematologic Malignancies. *Journal of Hematology and Oncology*. BioMed Central Ltd July 27, 2020. https://doi.org/10.1186/s13045-020-00924-z.

(12) Lai, A. C.; Toure, M.; Hellerschmied, D.; Salami, J.; Jaime-Figueroa, S.; Ko, E.; Hines, J.; Crews, C. M. Modulares PROTAC-Design Zum Abbau von Onkogenem BCR-ABL. *Angewandte Chemie* **2016**, *128* (2), 818–821. https://doi.org/10.1002/ange.201507634.

(13) Schneekloth, A. R.; Pucheault, M.; Tae, H. S.; Crews, C. M. Targeted Intracellular Protein Degradation Induced by a Small Molecule: En Route to Chemical Proteomics. *Bioorg Med Chem Lett* **2008**, *18* (22), 5904–5908. https://doi.org/10.1016/j.bmcl.2008.07.114.

(14) Lee, H.; Puppala, D.; Choi, E. Y.; Swanson, H.; Kim, K. B. Targeted Degradation of the Aryl Hydrocarbon Receptor by the PROTAC Approach: A Useful Chemical Genetic Tool. *ChemBioChem* **2007**, *8* (17), 2058–2062. https://doi.org/10.1002/cbic.200700438.

(15) Zhou, C.; Fan, Z.; Gu, Y.; Ge, Z.; Tao, Z.; Cui, R.; Li, Y.; Zhou, G.; Huo, R.; Gao, M.; Wang, D.; He, W.; Zheng, M.; Zhang, S.; Xu, T. Design, Synthesis, and Biological Evaluation of Potent and Selective PROTAC Degraders of Oncogenic KRASG12D. *J Med Chem* **2023**. https://doi.org/10.1021/acs.jmedchem.3c01622.

(16) Tang, R.; Wang, Z.; Xiang, S.; Wang, L.; Yu, Y.; Wang, Q.; Deng, Q.; Hou, T.; Sun, H. Uncovering the Kinetic Characteristics and Degradation Preference of PROTAC Systems with Advanced Theoretical Analyses. *JACS Au* **2023**, *3* (6), 1775–1789. https://doi.org/10.1021/jacsau.3c00195.

(17) Burslem, G. M.; Crews, C. M. Small-Molecule Modulation of Protein Homeostasis. *Chemical Reviews*. American Chemical Society September 13, 2017, pp 11269–11301. https://doi.org/10.1021/acs.chemrev.7b00077.

(18) Sun, X.; Gao, H.; Yang, Y.; He, M.; Wu, Y.; Song, Y.; Tong, Y.; Rao, Y. Protacs: Great Opportunities for Academia and Industry. *Signal Transduction and Targeted Therapy*. Springer Nature 2019. https://doi.org/10.1038/s41392-019-0101-6.

(19) Roy, M. J.; Winkler, S.; Hughes, S. J.; Whitworth, C.; Galant, M.; Farnaby, W.; Rumpel, K.; Ciulli, A. SPR-Measured Dissociation Kinetics of PROTAC Ternary Complexes Influence Target Degradation Rate. *ACS Chem Biol* **2019**, *14* (3), 361–368. https://doi.org/10.1021/acschembio.9b00092.

(20) Gadd, M. S.; Testa, A.; Lucas, X.; Chan, K. H.; Chen, W.; Lamont, D. J.; Zengerle, M.; Ciulli, A. Structural Basis of PROTAC Cooperative Recognition for Selective Protein Degradation. *Nat Chem Biol* **2017**, *13* (5), 514–521. https://doi.org/10.1038/nchembio.2329.

(21) Zorba, A.; Nguyen, C.; Xu, Y.; Starr, J.; Borzilleri, K.; Smith, J.; Zhu, H.; Farley, K. A.; Ding, W. D.; Schiemer, J.; Feng, X.; Chang, J. S.; Uccello, D. P.; Young, J. A.; Garcia-Irrizary, C. N.; Czabaniuk, L.; Schuff, B.; Oliver, R.; Montgomery, J.; Hayward, M. M.; Coe, J.; Chen, J.; Niosi, M.; Luthra, S.; Shah, J. C.; El-Kattan, A.; Qiu, X.; West, G. M.; Noe, M. C.; Shanmugasundaram, V.; Gilbert, A. M.; Brown, M. F.; Calabrese, M. F. Delineating the Role of Cooperativity in the Design of Potent PROTACs for BTK. *Proc Natl Acad Sci U S A* **2018**, *115* (31), E7285–E7292. https://doi.org/10.1073/pnas.1803662115.

(22) Drummond, M. L.; Williams, C. I. In Silico Modeling of PROTAC-Mediated Ternary Complexes: Validation and Application. *J Chem Inf Model* **2019**, *59* (4), 1634–1644. https://doi.org/10.1021/acs.jcim.8b00872.

(23) Bai, N.; Miller, S. A.; Andrianov, G. V.; Yates, M.; Kirubakaran, P.; Karanicolas, J. Rationalizing PROTAC-Mediated Ternary Complex Formation Using Rosetta. *J Chem Inf Model* **2021**, *61* (3), 1368–1382. https://doi.org/10.1021/acs.jcim.0c01451.

(24) Zaidman, D.; Prilusky, J.; London, N. ProsetTac: Rosetta Based Modeling of PROTAC Mediated Ternary Complexes. *J Chem Inf Model* **2020**, *60* (10), 4894–4903. https://doi.org/10.1021/acs.jcim.0c00589.

(25) Drummond, M. L.; Henry, A.; Li, H.; Williams, C. I. Improved Accuracy for Modeling ProTAC-Mediated Ternary Complex Formation and Targeted Protein Degradation via New in Silico Methodologies. *J Chem Inf Model* **2020**, *60* (10), 5234–5254. https://doi.org/10.1021/acs.jcim.0c00897.

(26) Ignatov, M.; Jindal, A.; Kotelnikov, S.; Beglov, D.; Posternak, G.; Tang, X.; Maisonneuve, P.; Poda, G.; Batey, R. A.; Sicheri, F.; Whitty, A.; Tonge, P. J.; Vajda, S.; Kozakov, D. High Accuracy Prediction of PROTAC Complex Structures. *J Am Chem Soc* **2023**, *145* (13), 7123–7135. https://doi.org/10.1021/jacs.2c09387.

(27) Schiemer, J.; Horst, R.; Meng, Y.; Montgomery, J. I.; Xu, Y.; Feng, X.; Borzilleri, K.; Uccello, D. P.; Leverett, C.; Brown, S.; Che, Y.; Brown, M. F.; Hayward, M. M.; Gilbert, A. M.; Noe, M. C.; Calabrese, M. F. Snapshots and Ensembles of BTK and CIAP1 Protein Degrader Ternary Complexes. *Nat Chem Biol* **2021**, *17* (2), 152–160. https://doi.org/10.1038/s41589-020-00686-2.

(28) Harada, R.; Shigeta, Y. Hybrid Cascade-Type Molecular Dynamics with a Markov State Model for Efficient Free Energy Calculations. *J Chem Theory Comput* **2019**, *15* (1), 680–687. https://doi.org/10.1021/acs.jctc.8b00802.

(29) Harada, R.; Kitao, A. Parallel Cascade Selection Molecular Dynamics (PaCS-MD) to Generate Conformational Transition Pathway. *Journal of Chemical Physics* **2013**, *139* (3). https://doi.org/10.1063/1.4813023.

(30) Harada, R.; Nakamura, T.; Shigeta, Y. Sparsity-Weighted Outlier FLOODing (OFLOOD) Method: Efficient Rare Event Sampling Method Using Sparsity of Distribution. *J Comput Chem* **2016**, *37* (8), 724–738. https://doi.org/10.1002/jcc.24255.

(31) Harada, R.; Nakamura, T.; Takano, Y.; Shigeta, Y. Protein Folding Pathways Extracted by OFLOOD: Outlier Flooding Method. *J Comput Chem* **2015**, *36* (2), 97–102. https://doi.org/10.1002/jcc.23773.

(32) Chan, K. H.; Zengerle, M.; Testa, A.; Ciulli, A. Impact of Target Warhead and Linkage Vector on Inducing Protein Degradation: Comparison of Bromodomain and Extra-Terminal (BET) Degraders Derived from Triazolodiazepine (JQ1) and Tetrahydroquinoline (I-BET726) BET Inhibitor Scaffolds. *J Med Chem* **2018**, *61* (2), 504–513. https://doi.org/10.1021/acs.jmedchem.6b01912.

(33) Dennington, R.; Keith, T.; Millam, J.; Eppinnett, K.; Hovell, W. L.; Gilliland, R. GaussView, Version 3.0 (Semichem, Inc., Shawnee Mission, KS). **2003**.

(34) Maier, J. A.; Martinez, C.; Kasavajhala, K.; Wickstrom, L.; Hauser, K. E.; Simmerling, C. Ff14SB: Improving the Accuracy of Protein Side Chain and Backbone Parameters from Ff99SB. *J Chem Theory Comput* **2015**, *11* (8), 3696–3713. https://doi.org/10.1021/acs.jctc.5b00255.

(35) Jourgensen, W. L.; Chandrasekhar, J.; Madura, J. D.; Impey, R. W.; Klein, M. L. Comparison of Simple Potential Functions for Simulating Liquid Water. *J. Chem. Phys.* **1983**, *79*, 926–935. https://doi.org/10.1063/1.445869.

(36) Frisch, M. J.; Trucks, G. W.; Schlegel, H. B.; Scuseria, G. E.; Robb, M. A.; Cheeseman, J. R.; Scalmani, G.; Barone, V.; Petersson, G. A.; Nakatsuji, H.; Li, X.; Caricato, M.; Marenich, A. V.; Bloino, J.; Janesko, B. G.; Gomperts, R.; Mennucci, B.; Hratchian, H. P.; Ortiz, J. V.; Izmaylov, A. F.; Sonnenberg, J. L.; Williams-Young, D.; Ding, F.; Lipparini, F.; Egidi, F.; Goings, J.; Peng, B.; Petrone, A.; Henderson, T.; Ranasinghe, D.; Zakrzewski, V. G.; Gao, J.; Rega, N.; Zheng, G.; Liang, W.; Hada, M.; Ehara, M.; Toyota, K.; Fukuda, R.; Hasegawa, J.; Ishida, M.; Nakajima, T.; Honda, Y.; Kitao, O.; Nakai, H.; Vreven, T.; Throssell, K.; Montgomery, J. A. , Jr.; Peralta, J. E.; Ogliaro, F.; Bearpark, M. J.; Heyd, J. J.; Brothers, E. N.; Kudin, K. N.; Staroverov, V. N.; Keith, T. A.; Kobayashi, R.; Normand, J.; Raghavachari, K.; Rendell, A. P.; Burant, J. C.; Iyengar, S. S.; Tomasi, J.; Cossi, M.; Millam, J. M.; Klene, M.; Adamo, C.; Cammi, R.; Ochterski, J. W.; Martin, R. L.; Morokuma, K.; Farkas, O.; Foresman, J. B.; Fox, D. J. Gaussian 16. Revision C.01. Wallingford CT 2016.

(37) Wang, J.; Wolf, R. M.; Caldwell, J. W.; Kollman, P. A.; Case, D. A. *Development and Testing of a General Amber Force Field*; 2004; Vol. 25.

(38) Salomon-Ferrer, R.; Case, D. A.; Walker, R. C. An Overview of the Amber Biomolecular Simulation Package. *Wiley Interdiscip Rev Comput Mol Sci* **2013**, *3* (2), 198–210. https://doi.org/10.1002/wcms.1121.

(39) Hess, B.; Bekker, H.; Berendsen, H. J. C.; Fraaije, J. G. E. M. LINCS: A Linear Constraint Solver for Molecular Simulations. *J Comput Chem* **1997**, *18* (12), 1463–1472. https://doi.org/10.1002/(SICI)1096-987X(199709)18:12<1463::AID-JCC4>3.0.CO;2-H.

(40) Bussi, G.; Donadio, D.; Parrinello, M. Canonical Sampling through Velocity Rescaling. *Journal of Chemical Physics* **2007**, *126* (1). https://doi.org/10.1063/1.2408420.

(41) Bussi, G.; Parrinello, M. Stochastic Thermostats: Comparison of Local and Global Schemes. *Comput Phys Commun* **2008**, *179* (1–3), 26–29. https://doi.org/10.1016/j.cpc.2008.01.006.

(42) Bussi, G.; Zykova-Timan, T.; Parrinello, M. Isothermal-Isobaric Molecular Dynamics Using Stochastic Velocity Rescaling. *Journal of Chemical Physics* **2009**, *130* (7). https://doi.org/10.1063/1.3073889.

(43) Berendsen, H. J. C.; Postma, J. P. M.; van Gunsteren, W. F.; Dinola, A.; Haak, J. R. Molecular Dynamics with Coupling to an External Bath. *Journal of Chemical Physics* **1984**, *81(8)*, 3684–3690. https://doi.org/10.1063/1.448118.

(44) Van Der Spoel, D.; Lindahl, E.; Hess, B.; Groenhof, G.; Mark, A. E.; Berendsen, H. J. C. GROMACS: Fast, Flexible, and Free. *Journal of Computational Chemistry*. December 2005, pp 1701–1718. https://doi.org/10.1002/jcc.20291.

(45) Harada, R.; Shigeta, Y. On-the-Fly Specifications of Reaction Coordinates in Parallel Cascade Selection Molecular Dynamics Accelerate Conformational Transitions of Proteins. *J Chem Theory Comput* **2018**, *14* (6), 3332–3341. https://doi.org/10.1021/acs.jctc.8b00264.

(46) Hengphasatporn, K.; Harada, R.; Wilasluck, P.; Deetanya, P.; Sukandar, E. R.; Chavasiri, W.; Suroengrit, A.; Boonyasuppayakorn, S.; Rungrotmongkol, T.; Wangkanont, K.; Shigeta, Y. Promising SARS-CoV-2 Main Protease Inhibitor Ligand-Binding Modes Evaluated Using LB-PaCS-MD/FMO. *Sci Rep* **2022**, *12* (1). https://doi.org/10.1038/s41598-022-22703-1.

(47) Harada, R.; Morita, R.; Shigeta, Y. Free-Energy Profiles for Membrane Permeation of Compounds Calculated Using Rare-Event Sampling Methods. *J Chem Inf Model* **2023**, *63* (1), 259–269. https://doi.org/10.1021/acs.jcim.2c01097.

(48) Munei, Y.; Hengphasatporn, K.; Hori, Y.; Harada, R.; Shigeta, Y. Determination of the Association between Mesotrione Sensitivity and Conformational Change of 4-Hydroxyphenylpyruvate Dioxygenase via Free-Energy Analyses. *J Agric Food Chem* **2023**, *71* (24), 9528–9537. https://doi.org/10.1021/acs.jafc.3c01253.

(49) Harada, R.; Nakamura, T.; Shigeta, Y. Automatic Detection of Hidden Dimensions to Obtain Appropriate Reaction Coordinates in the Outlier FLOODing (OFLOOD) Method. *Chem Phys Lett* **2015**, *639*, 269–274. https://doi.org/10.1016/j.cplett.2015.09.031.

(50) Harada, R.; Nakamura, T.; Shigeta, Y. A Fast Convergent Simulated Annealing Algorithm for Protein-Folding: Simulated Annealing Outlier Flooding (Sa-Oflood) Method. *Bull Chem Soc Jpn* **2016**, *89* (11), 1361–1367. https://doi.org/10.1246/bcsj.20160244.

(51) Nakamura, T.; Kamidoi, Y.; Wakabayashi, S.; Yoshida, N. FlexDice: A Fast Clustering Method for Large High Dimensional Data Sets. *IPSJ Transactions on Databases* **2005**, *46* (18), 40–49.

(52) Chodera, J. D.; Noé, F. Markov State Models of Biomolecular Conformational Dynamics. *Current Opinion in Structural Biology*. Elsevier Ltd 2014, pp 135–144. https://doi.org/10.1016/j.sbi.2014.04.002.

(53) Scherer, M. K.; Trendelkamp-Schroer, B.; Paul, F.; Pérez-Hernández, G.; Hoffmann, M.; Plattner, N.; Wehmeyer, C.; Prinz, J. H.; Noé, F. PyEMMA 2: A Software Package for Estimation, Validation, and Analysis of Markov Models. *J Chem Theory Comput* **2015**, *11* (11), 5525–5542. https://doi.org/10.1021/acs.jctc.5b00743.

(54) Massova, I.; Kollman, P. A. *Combined Molecular Mechanical and Continuum Solvent Approach (MM-PBSA/GBSA) to Predict Ligand Binding*; KLUWER/ESCOM, 2000; Vol. 18.

(55) Valdés-Tresanco, M. S.; Valdés-Tresanco, M. E.; Valiente, P. A.; Moreno, E. Gmx_MMPBSA: A New Tool to Perform End-State Free Energy Calculations with GROMACS. *J Chem Theory Comput* **2021**, *17* (10), 6281–6291. https://doi.org/10.1021/acs.jctc.1c00645.

(56) Crowe, C.; Nakasone, M. A.; Chandler, S.; Tatham, M. H.; Makukhin, N.; Hay, R. T.; Ciulli, A. Mechanism of Degrader-Targeted Protein Ubiquitinability. https://doi.org/10.1101/2024.02.05.578957.